Int J Adv Manuf Technol (2018) 94:2763–2771
DOI 10.1007/s00170-017-1052-0

ORIGINAL ARTICLE

Method for producing porosity-free joints in laser beam welding of maraging steel 250

Reuven Katz[1] · **Anton Zak**[1] · **Amnon Shirizly**[2] · **Amiram Leitner**[2] · **Elie Louzon**[2]

Received: 3 July 2017 / Accepted: 6 September 2017 / Published online: 18 September 2017

Abstract Laser beam welding of 4.5-mm-thick sheets of maraging steel 250 using a 4-kW ytterbium fiber laser was studied. Maraging steel 250 is widely used in the aerospace industry in applications that require high strength. Therefore, in order to join two parts made of maraging steel 250, it is essential to produce a high-quality weld that meets weld bead geometry requirements, without any porosity formation in the weld that may lead to premature fatigue failure. In order to achieve a reliable and repeatable welding process, we investigated the influence of welding parameters on the welded process responses, i.e., weld penetration depth, bead width, and potential formation of porosity. A complete model was developed using multiple regression analysis. Based on this model, we developed a method for selecting welding parameters that assure production of porosity-free welds with the required geometry. We used this method to automate the industrial welding process of a part-family of maraging steel 250 cylinders.

Keywords Laser beam welding · Porosity formation · Weld bead geometry · Multiple regression analysis

Nomenclature

LP	Laser power, W
S	Welding speed, m/min
F	Focal depth, mm
TET	Shield gas tilt, mm
D	Focal diameter, mm
CM	Workpiece cleanness
N	Shield gas nozzle distance, mm
WW	Weld width, mm
PD	Penetration depth, mm
POR	Porosity, %
CM	Workpiece cleanness level (1, 2, 3)

1 Introduction

Laser beam welding (LBW) has become a reliable and robust industrial process for joining mechanical elements [1]. LBW is characterized by a narrow weld width and high penetration, a narrow heat-affected zone, and minimal distortion of the workpiece. These advantages come from the high power density of the laser beam. The geometry of the laser weld bead and its quality are determined by the selected combination of input parameters. The main input parameters that control process quality are laser power, welding speed, focal depth, and shielding gas [2].

Norris et al. [3] studied the effect of welding parameters on porosity formation in hot rolled 304-L stainless steel thin

✉ Reuven Katz
reuvenk@technion.ac.il

Anton Zak
sushkin30@gmail.com

Amnon Shirizly
amnons@rafael.co.il

Amiram Leitner
amiraml@rafael.co.il

Elie Louzon
elilo@rafael.co.il

[1] Department of Mechanical Engineering, Technion, 32000 Technion City, Haifa, Israel

[2] Rafael – Advanced Defense Systems Ltd., P.O.B 2250, 3102102 Haifa, Israel

sheets. One of their findings was that weld porosity could result in a loss of weld strength or premature fatigue failure. The risk of weld failure depends upon the magnitude and type of loading forces, the environment, the severity of the porosity, and the type of material. Maraging steel 250 is widely used in aerospace applications, where reliability is critical and weld porosity cannot be accommodated. Gouret et al. [4] studied porosity caused by electron beam welding (EBW) of a TA6V alloy and reported that the cleanness level of the welded surface influences the appearance and the level of porosity in the weld. Haboudoua et al. [5] came to a similar conclusion in laser welding of aluminum alloys. Also, in our study of porosity formation in LBW of maraging steel 250, surface cleanness was included as a parameter. It is important to note that cleanness level is a discrete parameter, unlike other selected parameters which are continuous. Ascari et al. [6] studied the effect of welding process parameters in laser-GMAW on porosity reduction in AA6082 aluminum 8-mm-thick plates. They found that welding current influences porosity formation. Norris et al. [3] stated that parameters such as weld size, laser power, material type, and weld joint geometry impact laser keyhole evolution and porosity formation.

To evaluate porosity in a welded joint, typically, an X-ray image of this surface is created. When the size and location of an individual pore are of interest, one of many "image segmentation methods" may be applied [7]. When porosity levels, or the percentage of pores within a given welded joint, are of interest, the "gray level method," which uses a gray level histogram of the image, may be applied [8]. To develop our model, we applied multiple regression analysis (MRA). Wu and Ume [9] applied stepwise regression analysis to predict penetration depth of butt welds in thin plates. Lee and Um [10] modeled a gas metal arc welding process by using the multiple regression analysis and neural network. Benyounis et al. [11] applied linear regression to model welding parameters to predict four responses: heat input, weld width, weld penetration, and the geometry of the heat-affected zone. Several authors proposed using the artificial neural network technique for modeling weld geometry of various materials and welding processes [12–14].

The goal of the study was developing a practical method for predicting welding parameters for producing porosity-free welds using an experimental method and a statistical analysis. The method can be applied when the user knows a priori what the "part-family" of products he intends to produce is. For this specific production process, one can apply our method and design an experimental plan with minimum needed experiments and find the welding parameters that promise high-quality, porosity-free welds.

In the study, an experimental plan was developed using a D-optimal design method. Twenty-three welding experiments and an additional three validation experiments were performed. Seven laser input parameters were taken into consideration: laser power, welding speed, focal depth, focal diameter, shield gas nozzle distance from the workpiece, shield gas tilt angle, and the cleanness level of the workpiece's surface. A complete model was developed based on the measured experimental data, applying the MRA method. This model was used to develop a practical algorithm that can be used to select parameters that assure the production of porosity-free welds to meet specific weld penetration and weld width requirements.

2 Experimental design

The experiment was planned using D-optimal design [15]. The D-optimality criterion seeks to maximize the determinant of the information matrix $X'X$ of a specific experiment design. The independent input variables and their values are presented in Table 1.

Second-order polynomials were fitted to the experimental data to obtain the regression equations. The general expression of the second-order polynomials [16] is presented in Eq. 1.

$$Y = b_0 + \sum b_i X_i + \sum b_{ii} X^2{}_{ii} + \sum b_{ij} X_i X_j \tag{1}$$

A multivariate regression method was applied to fit this explicit expression to the experimental data to identify the required b_{ij} coefficients [16]. In order to reduce the number of required experiments out of the 21 terms included in the expression $\sum b_{ij} X_i X_j$, we used only seven terms, which were selected based on our welding and statistics experts' experience and knowledge. For example, CM is a qualitative parameter (represents surface cleanness level) and not a continuous numerical parameter as all other parameters. The term CM^2 does not have a meaning and adding it will not add information; therefore, it was left out. The modified equation is presented in Eq. 2.

$$\begin{aligned} Y = {} & b_1 + b_2{\cdot}LP + b_3{\cdot}S + b_4{\cdot}F + b_5{\cdot}TET + b_6{\cdot}D \\ & + b_7{\cdot}CM + + b_8{\cdot}N + b_9{\cdot}LP^2 + b_{10}{\cdot}S^2 + b_{11}{\cdot}F^2 \\ & + b_{12}{\cdot}TET^2 + b_{13}{\cdot}D^2 + + b_{14}{\cdot}N^2 + b_{15}{\cdot}D{\cdot}S \\ & + b_{16}{\cdot}N{\cdot}D + b_{17}{\cdot}N{\cdot}F + b_{18}{\cdot}LP{\cdot}CM + b_{19}{\cdot}S{\cdot}F \\ & + b_{20}{\cdot}S{\cdot}LP + b_{21}{\cdot}N{\cdot}LP \end{aligned} \tag{2}$$

Table 1 Measured welding parameters and their levels

Parameter	Code	Unit	L1	L2	L3
Laser power	LP	W	1000	2000	3000
Welding speed	*S*	m/min	2	3	5
Focal depth	*F*	mm	0	1.5	3
Shield gas tilt	TET	deg	20	–	30
Focal diameter	*D*	mm	0.378	0.513	0.693
Workpiece cleanness	CM	–	None	Acetone	Polish + acetone
Shield gas distance	*N*	mm	6	10	15

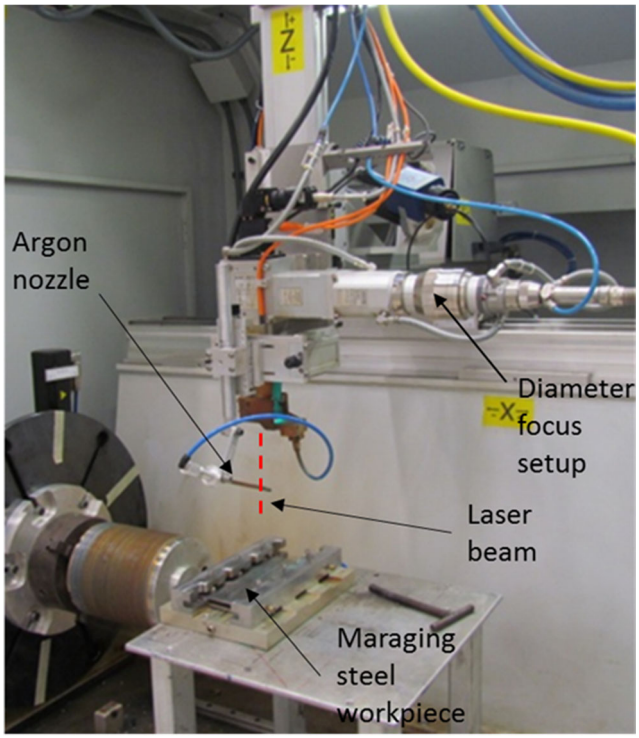

Fig. 1 Experimental setup

3 Experimental method and results

Maraging steel 250 with chemical nominal composition in weight percent of 18.46% Ni, 8.3% Co, 4.7% Mo, 0.45% Ti, 0.1% Al, 0.01% C, and Fe balance was used as workpiece material. The size of each plate was 200 × 100 mm and its thickness was 4.5 mm. The experiment was performed according to the design table in random order to avoid systematic errors. The experiments were carried out using 4-kW ytterbium fiber laser, model YLS-4000-CT-WW from IPG Laser GmbH. Pure argon was used as the shielding gas. The experimental setup is presented in Fig. 1.

Two transverse specimens were cut from each weld. A standard metallographic cross section was made for each transverse specimen. The bead profile geometry, i.e., penetration and width, was measured using an optical microscope. An integrated software package that amplifies the image ×100 allows measurement of weld bead dimensions within 0.001-mm accuracy. The average of two measured profile parameters was logged for each experiment. Two examples of bead geometry cross sections are shown in Fig. 2. On the left is a typical cross section for a low laser power and low welding speed weld. On the right is a typical cross section for a high laser power and high welding speed weld.

The porosity formed in the welded joint is shown in Fig. 3. The image was taken using a Microfocus X-Ray camera and VisiView image processing software, from Vistron Systems GmbH. The image was analyzed using MATLAB, and each pixel received a gray level value between 0 and 255, where 0 represents the black pixels and 255 represents the white pixels. Porosity is represented by dark pixels. Applying the gray level method [8], a histogram of all pixels located within the area outlined by the rectangle in Fig. 3 was created; the histogram is shown in Fig. 4. Zone II, which is located to the right of the graph minimum, represents the dark pixels of porosity, while zone I represents the rest of the welded area without porosity. We estimated porosity percentage in the welded joint by dividing the number of pixels located in zone II by the total number of pixels under the curve.

During the welding process, *heat input* to the workpiece is produced by the laser beam, and it depends on welding speed. The value of heat input can be calculated for each experiment, since heat input = $\eta \times (LP/S)$, where η, energy transfer efficiency, is in the range of 0.7–0.8 [17], and both L and S are known input parameters.

The experiments were performed in a random order following the optimal design matrix shown in Table 2. Table 2 also includes the measured results obtained from the 23

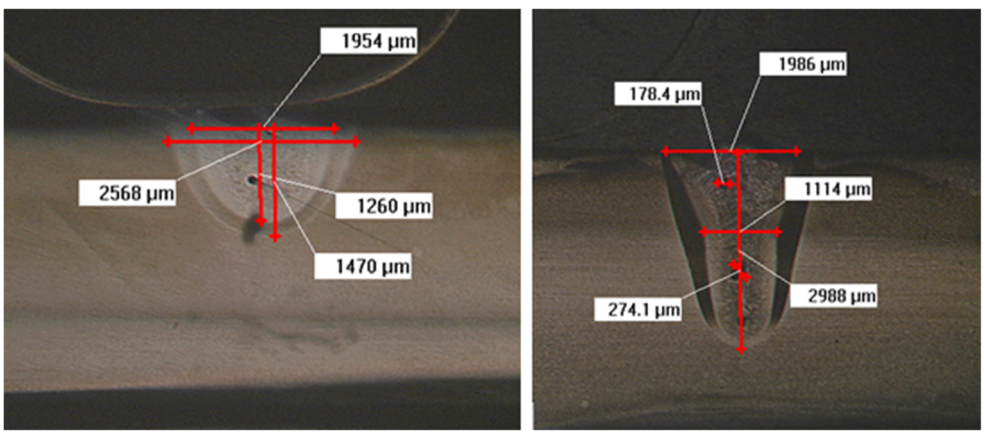

Fig. 2 Measured bead geometry (on the left: low power and low welding speed weld; on the right: high power and high welding speed weld)

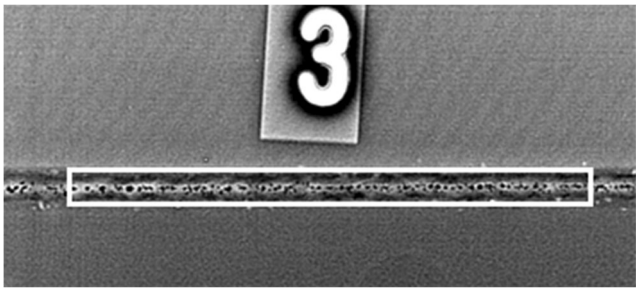

Fig. 3 Porosity in welded joint (experiment 3) and the area analyzed

welding experiments: weld penetration depth, weld bead width, and the percentage of porosity in the weld.

The responses of weld bead geometry were measured using transverse sectioned specimens and an optical microscope. Porosity was measured using the gray level method as described earlier in this section.

4 Modeling weld bead geometry

The weld bead geometry i.e., depth of penetration and weld bead width, were modeled using multiple regression analysis (MRA).

4.1 MRA

The modified quadratic model in Eq. 2 was used to fit the experimental responses listed in Table 2. We tested the significance of the regression models, the significance of individual model coefficients, and lack of fit utilizing ANOVA with JMP 13 statistical software. The multivariate regression method designates which are the significant parameters in the model.

4.1.1 Penetration depth

Figure 5 presents the fit between the predicted and actual values. The predicted values were calculated using the penetration depth model in Eq. 3, and the actual values represent the 23 experimental results in Table 2. R^2 = 0.95, RMSE = 0.276, and P value <0.0001 represent a very good fit between the predicted and actual responses.

$$\textit{Penetration depth}\ (\text{mm}) = 2.0089 + 0.0011\ LP - 0.3510\ S - 1.4471\ D - 1.0289 \times 10^{-4}(LP - 1956.5217)(S - 3.3043) \quad (3)$$

Equation 3 shows that as increasing laser power increases heat input to the workpiece, more metal volume is molten, therefore increasing penetration depth. Increasing welding speed (S) decreases heat input, and as result, decreases weld penetration. Decreasing the focal diameter (D) increases the laser power density, which means that the heat will localize in a small metal area, and therefore, penetration depth increases. To achieve maximum penetration depth, one should increase LP and decrease S and D. Benyounis et al. [11] presented an empirical relation of weld penetration that depends on the parameters LP, S, and F.

4.1.2 Weld bead width

Figure 5 (on the right) shows the fit between the predicted and actual values of weld bead width. The predicted values were calculated using the weld zone width model according to Eq. 4, and the actual measured values are from Table 3. R^2 = 0.91, RMSE = 0.243, and P value <0.0001 represent a good fit between predicted and actual responses. The empirical model for weld bead width is presented in Eq. 4.

$$\textit{Weld bead width}\ (\text{mm}) = 2.0485 + 6.0663 \times 10^{-4}\ \text{LP} - 0.3176\ S - 1.3335 \times 10^{-4}(\text{LP} - 1956.5217)(S - 3.3043) \quad (4)$$

Equation 4 shows that increasing laser power LP increases the weld zone width. Conversely, increasing the welding speed decreases weld zone width.

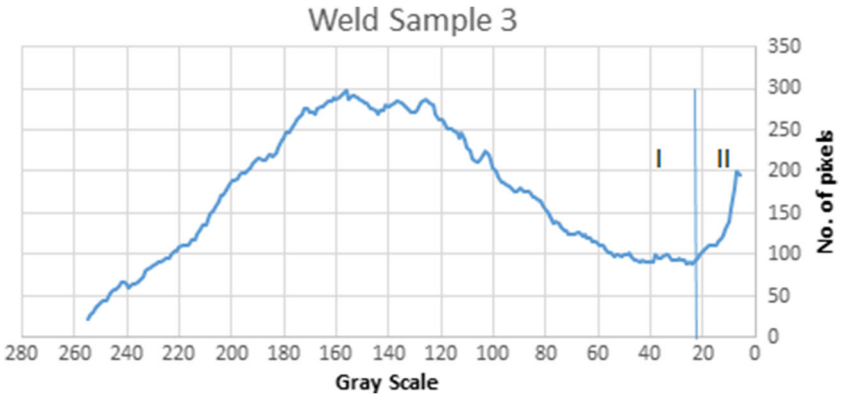

Fig. 4 Histogram of the gray scale representing all pixels within the rectangle in Fig. 3

Table 2 Experimental design matrix and experimental responses

Welding parameters							Measured result		
LP (W)	*S* (m/min)	*F* (mm)	TET (deg)	*D* (mm)	CM	*N* (mm)	Porosity (%)	Penetration depth	Weld width
2000	3	1.5	20	0.378	L1	10	1.5	2.565	2.513
2000	2	0	30	0.513	L3	15	0.4	2.64	2.23
1000	2	0	30	0.378	L1	6	4.2	1.97	1.961
1000	5	0	30	0.693	L3	15	0	0.633	1.16
2000	5	0	30	0.693	L2	6	0	1.209	2.08
1000	2	1.5	30	0.693	L2	15	0	1.127	1.75
1000	5	0	20	0.513	L2	10	0	0.97	1.28
1000	2	3	20	0.693	L1	15	0	1.071	1.924
3000	3	3	30	0.513	L2	6	1.4	3.34	2.8
3000	2	3	30	0.378	L1	15	0.4	4.182	3.78
3000	5	3	30	0.378	L3	10	0.18	2.78	1.96
1000	5	3	30	0.693	L1	6	0	0.541	1.275
1000	2	3	30	0.378	L3	10	0.07	1.804	1.813
1000	5	3	20	0.378	L2	15	0	0.8	1.22
3000	2	1.5	30	0.693	L1	6	0.51	4.074	3.637
1000	2	0	20	0.693	L3	6	0	1.13	1.73
3000	2	1.5	20	0.378	L3	6	2.9	3.93	3.02
3000	5	0	20	0.513	L1	6	2.7	2.867	2.053
2000	2	3	20	0.513	L2	6	0.8	3.068	3.084
3000	5	1.5	30	0.513	L2	15	0.02	2.65	2.043
3000	*3*	*3*	*20*	*0.693*	*L3*	*15*	*0*	*3.026*	*2.624*
3000	2	0	20	0.693	L2	10	0.32	4.2	3.46
1000	5	1.5	20	0.378	L3	6	0.23	1.127	1.241

The italic values in the table are presented later in the example, section 7.3.2

5 Modeling porosity formation in a welded joint

The MRA method provided a model with outstanding fit between the predicted and actual values for porosity response (Fig. 6). The predicted values were calculated using the porosity model according to Eq. 5, and the actual measured values are presented in Table 2. $R^2 = 0.99$, RMSE = 1.471, and P value <0.0001 represent an excellent fit between predicted and measured responses.

ANOVA revealed that six out of the seven selected parameters, with the exception of the shield gas tilt angle (TET), have significant effect on porosity formation, as presented in Eq. 5. The equation for predicting porosity formation in the weld is written in a concise form for the three levels of surface cleaning: no cleaning (L1), cleaning with acetone (L2), and using a pneumatic polisher to clean the surface (L3).

$$\begin{Bmatrix} Porosity\ (\%)\ \text{for CM (L1)} \\ Porosity\ (\%)\ \text{for CM (L2)} \\ Porosity\ (\%)\ \text{for CM (L3)} \end{Bmatrix} = \Big[3.5914 + 2.3926\times10^{-4}\ \text{LP} - 0.0569\ S - 0.1088\ F - 2.5370\ D - 0.1067\ N\Big]\begin{Bmatrix}1\\1\\1\end{Bmatrix} + \begin{Bmatrix}0.4436\\-0.0446\\-0.3989\end{Bmatrix} + \Big[0.4009(S-3.3043)(F-1.5652) + 3.4987(S-3.3043)(D-0.5364) - 35.6625(D-0.5364)(D-0.5364) - 8.4524\times10^{-5}(\text{LP}-1956.5217)(N-10) + 0.1028(F-1.5621)(N-10) + 1.396(D-0.5364)(N-10)\Big]\begin{Bmatrix}1\\1\\1\end{Bmatrix} + (\text{LP}-1956.5217)\times10^{-4}\begin{Bmatrix}3.7589\\-1.1308\\-2.6281\end{Bmatrix} \quad (5)$$

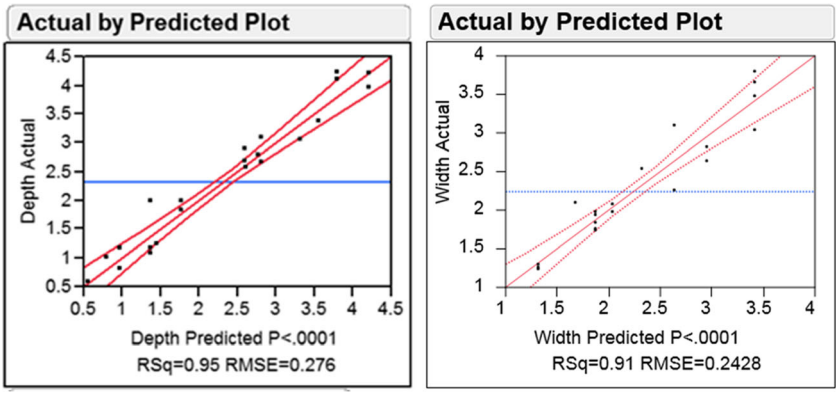

Fig. 5 Predicted vs. actual fit: penetration depth (left) and weld bead width (right)

Figure 7 presents the porosity prediction profiler, which clearly portrays the effect of each parameter on porosity formation. Increasing laser power (LP) increases porosity. Increasing welding speed (*S*) and focal depth (*F*) decreases porosity. The effect of focal diameter (*D*) has a quadratic shape, and in order to reduce porosity, a large focal diameter is preferred. The sixth significant parameter is surface cleanness (CM), and Fig. 7 shows that porosity formation is reduced as the surface is better cleaned or prepared. In Fig. 7, the values in red represent a weld with 1.8% porosity and the two blue lines represent a tolerance of 0.2%. We have no interest in this specific example; however, we are interested in observing the influence of each parameter on porosity formation. Haboudoua et al. [5] showed that improved surface preparation reduces porosity formation tendency in laser welding of aluminum alloys. Similar to our results, they showed that a polished surface is better than a degreased surface. In their study, they also welded sand-blasted surfaces and laser-cleaned surfaces that further reduced porosity formation. Norris et al. [3] studied laser welding of 304-L stainless steel with weld penetration depth under 2 mm. They reported that increased travel speed reduced porosity formation. In addition, their study found that pore size increased parabolically with laser heat input.

6 Experimental verification of the model

At the end of the 23 experiments required to find the model parameters, we performed an additional three experiments to verify the fit between the model and the actual measured values. Welding parameters as well as the measured responses are presented in Table 3. The errors presented in the table show good fit (under 10%) between the predicted values from the model and the experimental results. Please note that the reported error may originate not only from the model's prediction error but also from measurement errors. From a practical point of view, it is important to clearly identify a porosity-free weld. In the next section, we will show how to apply the developed model for producing porosity-free joints that meet weld geometry requirements.

7 A method for selecting welding parameters based on the model

As explained earlier, for aerospace applications, high-quality welds of maraging steel 250 must be porosity-free. We propose a method for evaluating welding parameters based on the developed model. The goal is to select a priori a set of welding

Table 3 Measured vs. predicted responses and relative errors

Experiment no.	LP (W)	*S* (m/min)	*F* (mm)	TET (deg)	*D* (mm)	CM (−)	*N* (mm)		Penetration (mm)	Width (mm)	Porosity (%)
								Measured	3.424	2.859	1.46
1	3000	3	3	30	0.513	L2	6	Predicted	3.561	2.956	1.49
								Error%	−4	−3.4	2
								Measured	1.270	1.890	0.00
2	1000	2	0	20	0.378	L3	6	Predicted	1.378	1.870	0.00
								Error%	−8.5	1.1	0
								Measured	4.118	3.650	0.42
3	3000	2	0	20	0.378	L2	10	Predicted	3.808	3.413	0.38
								Error%	7.5	6.5	9.5

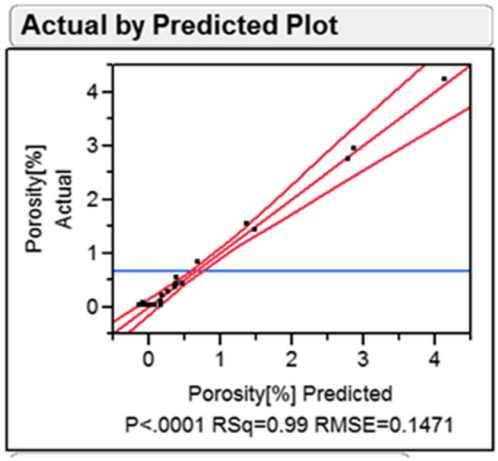

Fig. 6 Predicted vs. actual fit: porosity formation

parameters that will meet penetration depth and weld width requirements and will produce a porosity-free weld.

Figure 8 presents a flowchart of the calculation method based on the model, which includes two main steps. We explain the method in detail below.

7.1 Step 1: Selecting welding parameters that assure the required weld geometry

Following the guidelines presented in Fig. 8, we will select the largest value of focal diameter (*D*) that promises less porosity at the weld. Next,

1. We input the required penetration depth (PD) and weld width (WW).
2. Using Eqs. 3 and 4, we find the values of the LP and welding speed (*S*) that meet these requirements. These are presented graphically in the upper right triangles in Fig. 9.
3. The intersections of these (LP, S) values give a set of possible parameters.

Observing Fig. 7, we recommend selecting the lowest (LP) and largest (*S*) values for minimum porosity formation.

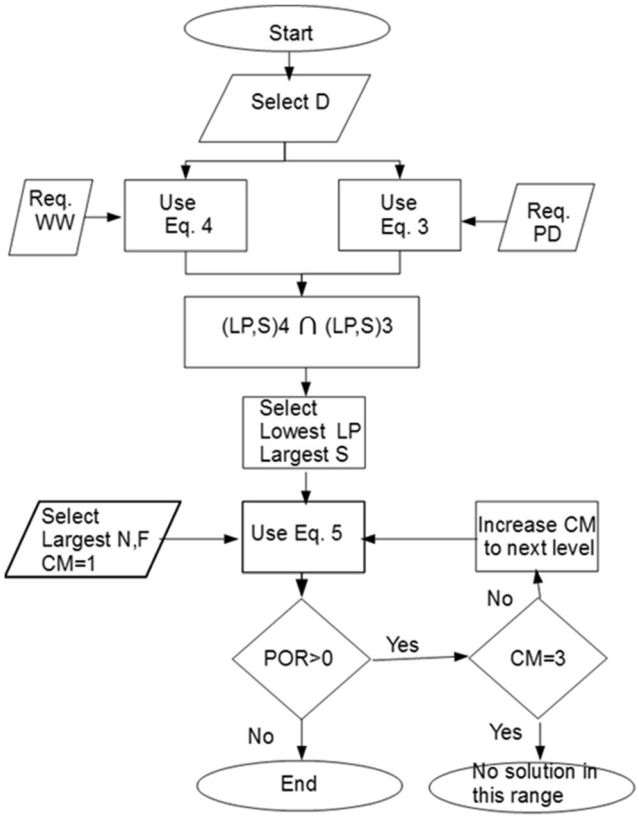

Fig. 8 Flowchart of the method for selecting welding parameters for a porosity-free weld

However, many other combinations may provide a porosity-free weld and meet the geometry requirement, as shown in the example in Sect. 7.3.

7.2 Step 2: Calculating the percentage of predicted porosity

1. The second step is related to evaluating the porosity percentage in the weld. Our goal is a porosity-free weld. We have to select the values of the distance between the inert gas nozzle and the surface (*N*) and focal depth (*F*). According to Fig. 9, largest values of both are recommended for reducing porosity formation. Please note that the above recommendation for selecting *N* and *F* is *only* valid for the range of parameters

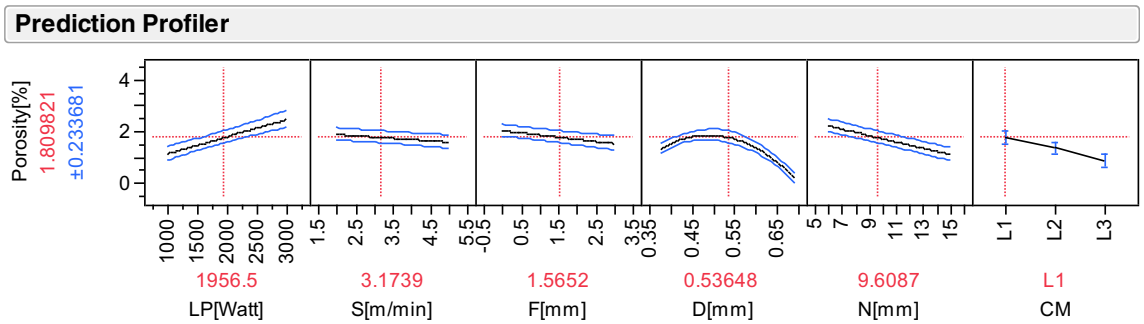

Fig. 7 The effect of welding parameters on porosity percentage

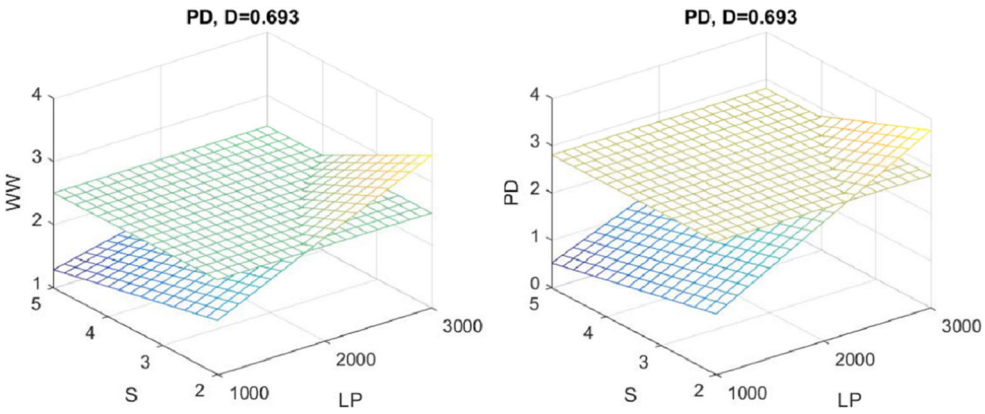

Fig. 9 Modeling weld bead geometry requirements (on the left: weld bead width; on the right: penetration depth)

tested in our experiments. For other sets of experimental parameters, recommendations may be different. For example, welders are interested in keeping the gas nozzle as close to the laser beam as possible to avoid oxidization of the welded surface. In our case, even at the largest distance, the gas protection is good.

2. We calculate Eq. 5 starting with the lowest value of surface cleanness, CM = 1, which represents a surface without any cleaning. If we calculate and find that porosity is expected in the weld, we increase CM to CM = 2, which represents surface cleaning with acetone. If we get a porosity-free weld, we stop the process and use the calculated parameters; otherwise, we increase CM to CM = 3, which represents a polished surface that has been cleaned with acetone, and recalculate Eq. 5. If we achieve a porosity-free weld as a result, we can use this set of welding parameters. If we cannot obtain a porosity-free weld even then, most probably, there is no suitable solution for the range of welding parameters that were selected for the experimental study, as shown in Table 1.

7.3 Example

The following numerical example will demonstrate how the model can be applied to assist the welding engineer in selecting parameters to achieve a porosity-free weld.

7.3.1 Example step 1

In the project specifications, the required weld geometry is given as penetration depth PD > 2.8 mm and weld width WW > 2.5 mm. We select $D = 0.693$ mm. Equations 3 and 4 are solved, and the expressions of PD and WW as a function of LP and S are presented graphically as the inclined surfaces in Fig. 9. The specified requirements are represented by the horizontal surface at each plot, respectively. The intersection between the surfaces provides the possible range of solutions for each requirement, which are represented by the upper right triangles in both plots of Fig. 9. We have to select LP and S values that satisfy both requirements, and we selected the values LP = 3000 W and $S = 3$ m/min.

7.3.2 Example step 2

Using the selected welding parameters in step 1, and further selecting $N = 15$ mm and $F = 3$ mm, we proceed to calculate Eq. 5, the percentage of porosity in the weld.

For CM = 1, surface without cleaning, POR(1) = 1.46%; for CM = 2, using acetone for surface cleaning, POR(2) = 0.46%; and finally, for CM = 3, which stands for surface polishing followed by acetone cleaning, POR(3) = 0% (porosity-free weld).

In summary, the selected parameters in this example allow us to produce a high-quality weld with the required geometry. Here, the selected parameters are LP = 3000 W, $S = 3$ m/min, $D = 0.693$ mm, $F = 3$ mm, $N = 15$ mm, and CM = 3.

Fig. 10 Production line (control room on the left and welding machine on the right)

Eventually, these welding parameters represent the input parameters of experiment no. 21 (italic font) in Table 2, where the penetration depth was measured to be 3.02 mm (>2.8 mm), the weld bead width was measured to be 2.62 mm (>2.5 mm), and POR(3) = 0%.

8 Industrial application

Due to global competition, the manufacturing industries are rapidly changing. New processes and new materials are being introduced. Much effort has been made to reduce costs by improving productivity and quality and by reducing production time through the use of automation and robots [18]. Introduction of computer-integrated manufacturing (CIM) means replacing manual work by automated work. Automated welding is taking over important manufacturing segments while the manual welding is being improved and modernized.

Our method was developed for improving the welding process and for reducing fabrication time of high-quality aerospace part-families. We planned to use this method for producing a part-family of products that required a welding process of two cylindrical parts made of maraging steel 250 with different diameters, but with a similar wall thickness. Although the experimental study was performed on plates, the goal of the industrial application was welding various cylinders. Applying the method saved manual trial-and-error work, which is typically needed for adjusting and selecting welding parameters for receiving high-quality welds. Part of the production line related to welding these cylinders is shown in Fig. 10.

9 Conclusions

1. The study presents a model based on multiple regression analysis that is capable of predicting weld bead geometry and porosity formation in the weld. The model was verified experimentally to show good fit with the predicted responses.
2. Based on the model, we established and demonstrated a practical method for selecting welding parameters that will produce a weld with specific geometry requirements and will be porosity-free, as required for high-quality maraging steel 250 welds.
3. The method requires minimum experimental effort for evaluating the best welding parameters for a porosity-free welding. Therefore, for high-quality automated welding application, it presents potential economic benefits.

Acknowledgements We would like to acknowledge the outstanding technical support from laser welding expert Mr. Benny Tavlovich and his team.

References

1. Schlueter H (2007) Laser beam welding: benefits, strategies, and applications. Weld J 86(5):37–39
2. Huang Q, Hagstroem J, Skoog H, Kullberg H (1991) Effect of laser parameter variation on sheet metal welding. Int J Join Mater 3(3): 79–88
3. Norris JT, Robino CV, Hirschfeld DA, Perricone MJ (2011) Effects of laser parameters on porosity formation: investigating millimeter scale continuous wave Nd:YAG laser welds. Weld J 90:198s–203s
4. Gouret N, Ollivier E, Dour G, Fortunier R, Miguet B (2004) Assessment of the origin of porosity in electron-beam-welded TA6V plates. Metall Mater Trans A 35(3):879–889. https://doi.org/10.1007/s11661-004-0013-z
5. Haboudou A, Peyre P, Vannes AB, Peix G (2003) Reduction of porosity content generated during Nd:YAG laser welding of A356 and AA5083 aluminum alloys. Mater Sci Eng A 363(1):40–52. https://doi.org/10.1016/s0921-5093(03)00637-3
6. Ascari A, Fortunato A, Orazi L, Campana G (2012) The influence of process parameters on porosity formation in hybrid laser-GMA welding of AA6082 aluminum alloy. Opt Laser Technol 44(5): 1485–1490. https://doi.org/10.1016/j.optlastec.2011.12.014
7. Steiner D, Katz R (2007) Measurements techniques of porosity flaws on machined surfaces. ASME J Comput Inf Sci Eng 7(1): 85–94. https://doi.org/10.1115/1.2424244
8. Taud H, Martinez-Angeles R, Parrot J, Hernandez-Escobedo L (2005) Porosity estimation method by X-ray computed tomography. J Pet Sci Eng 47(3):209–217. https://doi.org/10.1016/j.petrol.2005.03.009
9. Wu TY, Ume CI (2012) Prediction and experimental validation of penetration depth of butt welds in thin plates using superimposed laser sources. NDT&E Int 50:10–19. https://doi.org/10.1016/j.ndteint.2012.04.002
10. Lee J, Um K (2000) A comparison in a back-bead prediction of gas metal arc welding using multiple regression analysis and artificial neural network. Opt Laser Eng 34:149–158. https://doi.org/10.1016/s0143-8166(00)00097-x
11. Benyounis KY, Olabi AG, Hashmi MS (2005) Effect of laser welding parameters on the heat input and weld-bead profile. J Mater Process Technol 164–165:978–985. https://doi.org/10.1016/j.jmatprotec.2005.02.060
12. Ghosh A, Chattopadhyaya S, Sarkar PK (2007) Effects of input parameters on weld bead geometry of saw process. In: Proceedings of the International Conference on Mechanical Engineering (ICME 2007), Dhaka, Bangladesh. pp 29–31
13. Kim IS, Son JS, Kim IG, Kim JY, Kim OS (2003) A study on relationship between process variables and bead penetration for robotic CO_2 arc welding. Int J Mater Process Technol 136:139–145. https://doi.org/10.1016/s0924-0136(02)01126-3
14. Towsyfyan H, Davoudi G, Dehkordy BH, Kariminasab A (2013) Comparing the regression analysis and artificial neural network in modeling the submerged arc welding (SAW) process. Res J Appl Sci Eng Technol 5(9):2701–2706
15. Heredia-Langner A, Carlyle WM, Montogomery DC, Borror CM, Runger GC (2003) Genetic algorithms for the construction of D-optimal designs. J Qual Technol 35(1):28–46
16. Montgomery DC (2001) Design and analysis of experiments, 5th edn. John Wiley & Sons, New York, pp 436–440
17. Fuerschbach PW (1996) Measurement and prediction of energy transfer efficiency in laser welding. Weld J 75:24s–34s
18. Boekholt R (2000) The welding workplace: technology change and work management for global welding industry. Abington publishing, Cambridge, pp 5–8